Substrate-dependent dynamics of UDP-galactopyranose mutase: Implications for drug design

Leonardo Boechi,[1]* Cesar Augusto F. de Oliveira,[2] Isabel Da Fonseca,[3] Karina Kizjakina,[3] Pablo Sobrado,[3] John J. Tanner,[4] and J. Andrew McCammon[1,2]

[1]Department of Chemistry and Biochemistry, University of California San Diego, La Jolla, California

[2]Department of Pharmacology, Howard Hughes Medical Institute, University of California San Diego, La Jolla, California

[3]Department of Biochemistry, Virginia Tech, Blacksburg, Virginia 24061

[4]Departments of Chemistry and Biochemistry, University of Missouri-Columbia, Columbia, Missouri 65211

Abstract: *Trypanosoma cruzi* is the causative agent of Chagas disease, a neglected tropical disease that represents one of the major health challenges of the Latin American countries. Successful efforts were made during the last few decades to control the transmission of this disease, but there is still no treatment for the 10 million adults in the chronic phase of the disease. In *T. cruzi*, as well as in other pathogens, the flavoenzyme UDP-galactopyranose mutase (UGM) catalyzes the conversion of UDP-galactopyranose to UDP-galactofuranose, a precursor of the cell surface β-galactofuranose that is involved in the virulence of the pathogen. The fact that UGM is not present in humans makes inhibition of this enzyme a good approach in the design of new Chagas therapeutics. By performing a series of computer simulations of *T. cruzi* UGM in the presence or absence of an active site ligand, we address the molecular details of the mechanism that controls the uptake and retention of the substrate. The simulations suggest a modular mechanism in which each moiety of the substrate controls the flexibility of a different protein loop. Furthermore, the calculations indicate that interactions with the substrate diphosphate moiety are especially important for stabilizing the closed active site. This hypothesis is supported with kinetics measurements of site-directed mutants of *T. cruzi* UGM. Our results extend our knowledge of UGM dynamics and offer new alternatives for the prospective design of drugs.

Keywords: UDP-galactopyranose mutase; UGM; accelerated molecular dynamics; MD; inhibitor design
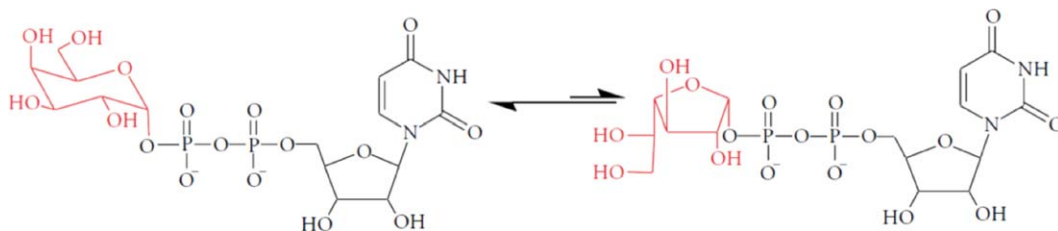
Figure 1. Non redox reaction catalyzed by UDP-galactopyranose mutase (UGM) to convert UDP-galactopyranose (UDP-Galp) to UDP-galactofuranose (UDP-Galf).[3] [Color figure can be viewed in the online issue, which is available at wileyonlinelibrary.com.]

Introduction

The protozoa parasite *Trypanosoma cruzi* is the causative agent of Chagas disease, which is one of the major health challenges of the American continents. The disease is associated with low socioeconomic rural areas where the most vulnerable part of the society is widely exposed to the vector *Triatoma infestans* that transmits the pathogen. Many fruitful efforts were made over the last years to control vectorial, congenital, and transfusional transmission.[1] The current treatment efforts are focused on infected adults. About 10 million people are infected and in the untreatable chronic phase of Chagas. The recent reports from the Pan American Health Organization (PAHO) emphasize the need for new drug treatment for chronic patients.[1] The drug benznidazol is currently used in Argentina, Brazil and Paraguay as a treatment for Chagas. Despite its side effects, this drug shows high efficacy in the first (acute) phase of the disease, especially in children under 5-year old.[2] Since the efficacy of benznidazol sharply decreases in young adults and older individuals, the development of new therapeutics for patients with symptoms of chronic Chagas disease is of great importance.

A promising new target against Chagas disease is the flavoenzyme UDP-galactopyranose mutase (UGM). UGM catalyzes the conversion of UDP-galactopyranose (UDP-Galp) to UDP-galactofuranose (UDP-Galf) (Fig. 1), a precursor of the cell surface compound β-galactofuranose (β-Galf) involved in the virulence of human prokaryotic pathogens such as *M. tuberculosis, E. coli, K. pneumoniae,* and eukaryotic pathogens such as *Leishmania spp, Aspergillus spp,* and *T. cruzi*.[3,4] The fact that UGM is not present in humans makes this enzyme a good target for therapeutics against these infectious diseases.

UGM uses flavin adenine dinucleotide (FAD) in the reduced form (FADH⁻) as a constitutive cofactor. Interestingly, the flavin does not participate in a net redox reaction, rather it acts as a nucleophile that attacks the anomeric carbon atom of the substrate. UGM is thus an example of a noncanonical flavoenzyme.[5]

Crystal structures are available for several UGMs. The *E. coli* UGM structure was reported in 2001 (PDB ID 1I8T),[6] and since then several more structures of bacterial and eukaryotic UGMs have been deposited in the Protein Data Bank. The portfolio of structures includes both oxidized and reduced enzymes as well as complexes with substrates and inhibitors (Table I). The overall folds of prokaryotic and eukaryotic UGMs are quite similar, however, eukaryotic UGMs are about 100 residues longer than the prokaryotic homologues. These extra residues form additional secondary structural elements, some of which are important for oligomerization and active site flexibility.[4] Thus, comparisons between the prokaryotic and eukaryotic UGMs should be made carefully.

Protein dynamics play a key role in substrate recognition by UGMs. For example, visual inspection of available crystal structures indicates that the absence of the substrate may be associated with an increased accessibility to the active site. Structures free of substrates (apo) display a tunnel-like topology for substrate migration to the active site, whereas structures that were co-crystallized with substrates or substrate analogues (holo) are completely closed (PDB ID 3UTF and PDB ID 3UTH, respectively). Two flaps are responsible for the opening/closing event, as illustrated by *Aspergillus fumigatus* (AfUGM). The 170s flap connects two helices in Domain 2 and corresponds to residues 179–187 of

Table I. *Crystal Structures of Reduced Eukaryotic UGMs*

Organism	Substrate	Tunnel volume (Å³)[a]	PDB ID	Observation
A. fumigatus	UDP-Galp	0.0	3UTH[7]−3UKF[38]	
A. fumigatus	UDP-Galp	0.0	3UKK[38]	Mutant R182K
A. fumigatus	UDP-Galp	0.0	3UKQ[38]	Mutant R327K
A. fumigatus	UDP-Galp	0.0	3UKP[38]	Mutant R327A
A. fumigatus	UDP	0.0	3UTG[7]−3UKL[38]	
A. fumigatus	Free	323–305	3UTF[7]−3UKA[38]	
T. cruzi	UDP	0.0	4DSH[8]	

[a] The tunnel volume was calculated with POVME software by using a representative subunit from each crystal structure.[34]
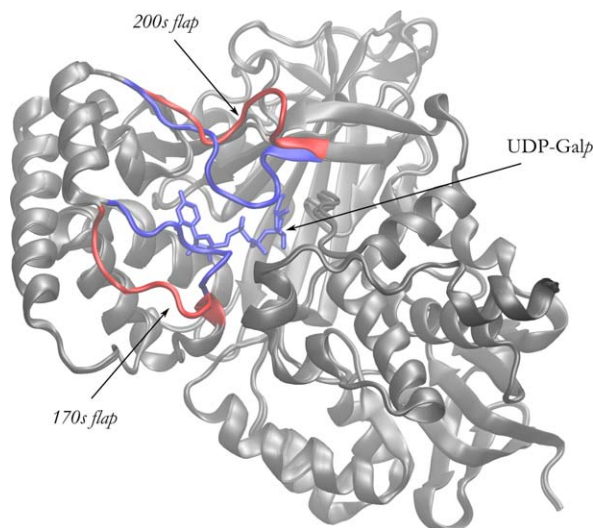
Figure 2. Crystal structures of the apo AfUGM (red)*(PDB ID 3UTF)* and holo AfUGM (blue)*(PDB ID 3UTH)* are superimposed. The natural substrate UDP-Gal*p* is also depicted (blue). [Color figure can be viewed in the online issue, which is available at wileyonlinelibrary.com.]

AfUGM and residues 173–181 of TcUGM. The 200s flap connects a helix from Domain 2 and a β-strand from Domain 1 (203–209 of AfUGM and 197–203 of TcUGM) (Fig. 2). Based on this structural data, an open/closed equilibrium depending on the absence/ presence of the substrate in the active site was proposed.[7] A new crystal structure of the holo *T. cruzi* UGM (TcUGM), depicting a closed-like state, was reported in 2012 and lends credence to the idea of an open/closed conformational equilibrium (PDB ID 4DSH). There is, however, no crystal structure available of the apo TcUGM (Table I).[8]

Several studies have been performed in recent years to identify UGM inhibitors.[9–16] These studies were performed with prokaryotic UGMs, mainly in *P. pneumoniae* and *M. tuberculosis* UGM, and no information about eukaryotic UGM inhibitors can be found in the literature. In many cases the small molecule inhibitors were largely designed based on substrate analogues that competitively bind to the active site, and only moderate inhibition could be achieved.[16] Moreover, the highly hydrophilic nature of the active site makes competitive drugs suboptimal from a pharmacokinetic point of view. New alternative inhibition mechanisms need to be explored in both prokaryotic and eukaryotic UGMs in order to strongly inhibit the enzyme. Leveraging protein dynamics is a promising approach for UGM drug design, although this hypothesis has not been formally explored, and the conformational changes attendant to substrate binding are still poorly characterized. A deeper understanding of the dynamic behavior of TcUGM and how it is affected by the presence of the substrate is of key importance in the design of more efficient drug screenings. In order to fulfill this goal, we have performed classical and accelerated molecular dynamics (MD) simulations to explore large-scale collective motions of the enzyme in both the presence and absence of UDP-Gal*p*, UDP, or uridine. Our results provide molecular details of TcUGM dynamics, which should aid in the development of future therapies for Chagas disease.

Results

Structure of the apo-TcUGM from MD and aMD simulations

To fully characterize the free form of TcUGM, we performed MD simulations of the apo enzyme using
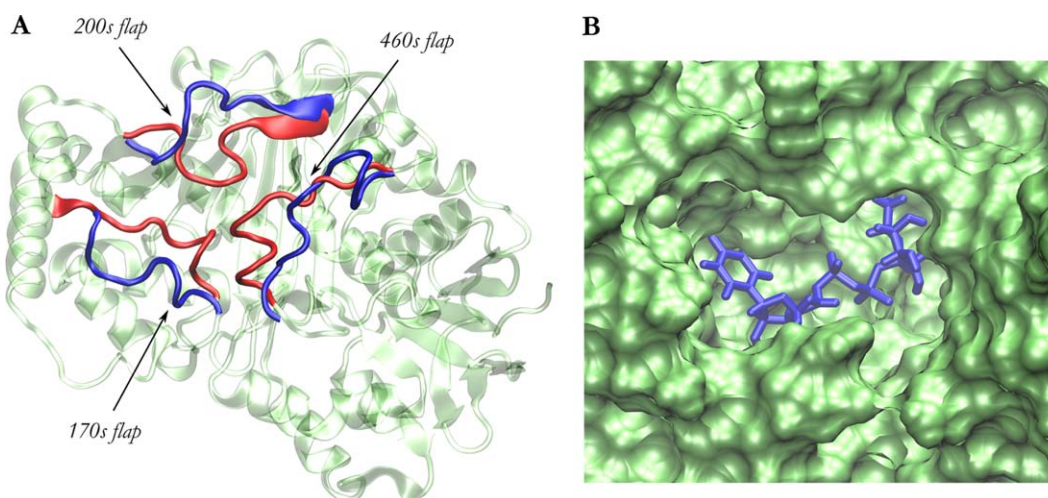

Figure 3. Secondary structure (A) and molecular surface (B) of the apo TcUGM model from MD simulations. The three flaps involved in the opening event before (red) and after (blue) MD were superimposed (A). The substrate UDP-Gal*p* (blue) was superimposed in the picture as a reference (B). http://imolecules3d.wiley.com:8080/imolecules3d/review/PeiUybyam4XULoE-foQSMa7IeILzkYlWZ8V8yUbY1CjTSPVJfdRHzBgnnIFKHAbAr711/1373. [Color figure can be viewed in the online issue, which is available at wileyonlinelibrary.com.]
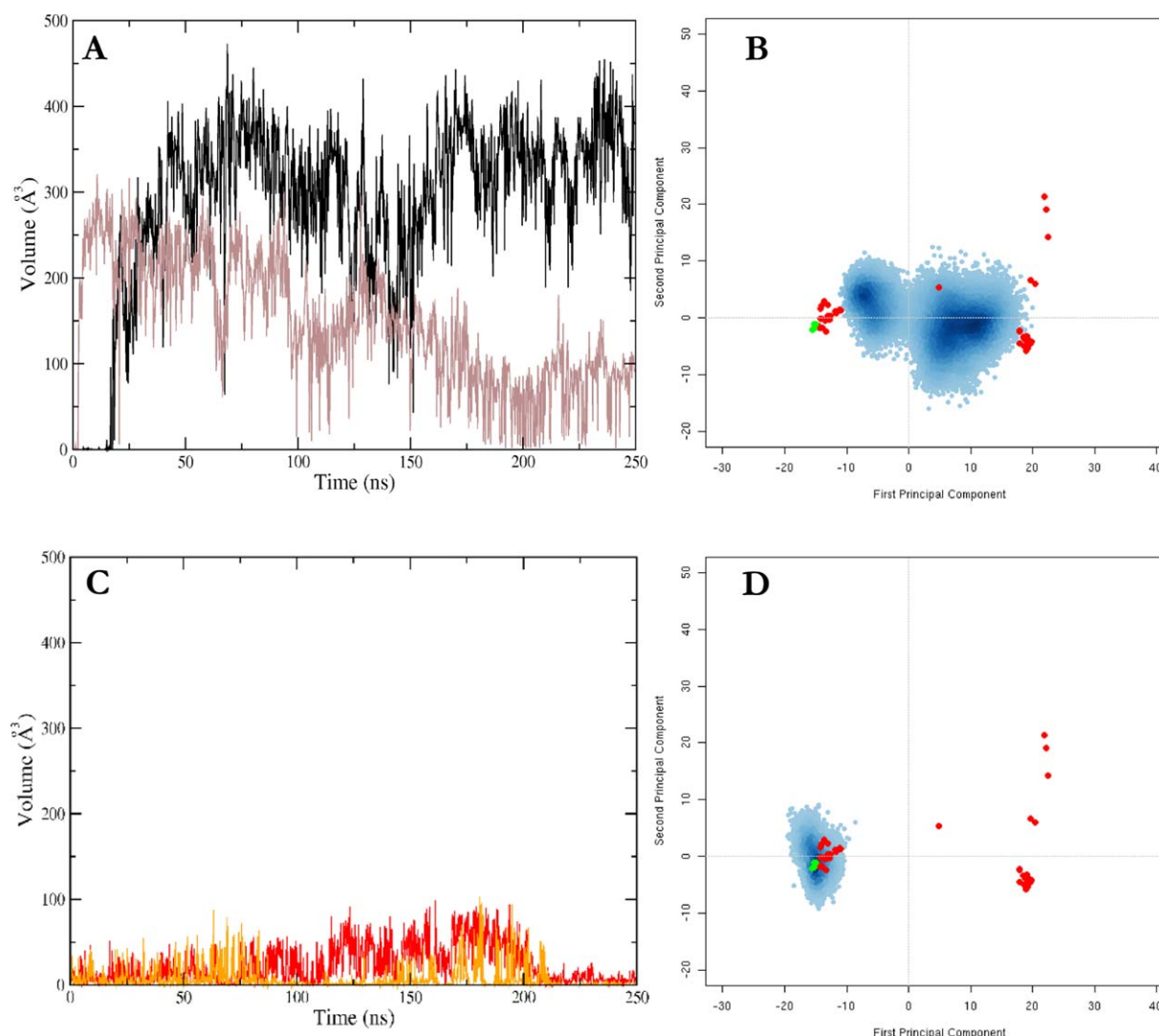
Figure 4. Channel volume and PC analysis for MD simulations of the apo (A and B, respectively) and holo (C and D, respectively) TcUGM. Two independent MD simulations were superimposed in the analysis (black and brown series in Panel A, red and orange colors in Panel B). PC analysis space built using all the AfUGM (red dots) and TcUGM (green dots) crystal structures. Dark regions in the PC space correspond to more populated configurations.

the atomic coordinates from the single available substrate-bound crystal structure of TcUGM (PDB ID 4DSH).[8] As a control, we performed MD simulations of the holo state, with the natural substrate UDP-Gal*p* in the active site. At the very beginning of the apo enzyme simulations both the 170s and 200s flaps move far apart, opening a clear channel that connects the solvent with the active site (Figs. 3 and 4). We also observed a third dynamic flap, which corresponds to residues 467–477 of AfUGM, and 461–471 of TcUGM, that occasionally increases the volume of the channel (Figs. 3 and 4).

The channel reaches volume values as large as the length of the substrate itself (Fig. 3B), suggesting that the channel is a suitable route for the substrate to reach the active site. The channel is occupied by water molecules and is topologically similar to the one observed in the crystal structure

of the *Aspergillus fumigatus* UGM (AfUGM) as well as in the prokaryotic UGMs (*E.coli, M. tuberculosis, K. pneumoniae*).

Volume analysis of the apo UGM channel identifies the opening of the tunnel at the beginning of two independent simulations (Fig. 4A). Both simulations show different behaviors: in the first simulation both flaps open widely and remain open during the entire simulation with volume values of around 37070 Å³ (Fig. 4A, black trace); in the second simulation, the 170s flap opens and then closes at the end of the simulation (Fig. 4A, brown trace), reaching values of around 110 ± 50 Å³. Noteworthy, the closing of the 170s flap still results in a conformation distinct from the crystal structure, as shown by an analysis of the principal components (PCs) of UGM dynamics, discussed in detail later. A third independent simulation shows similar result as the
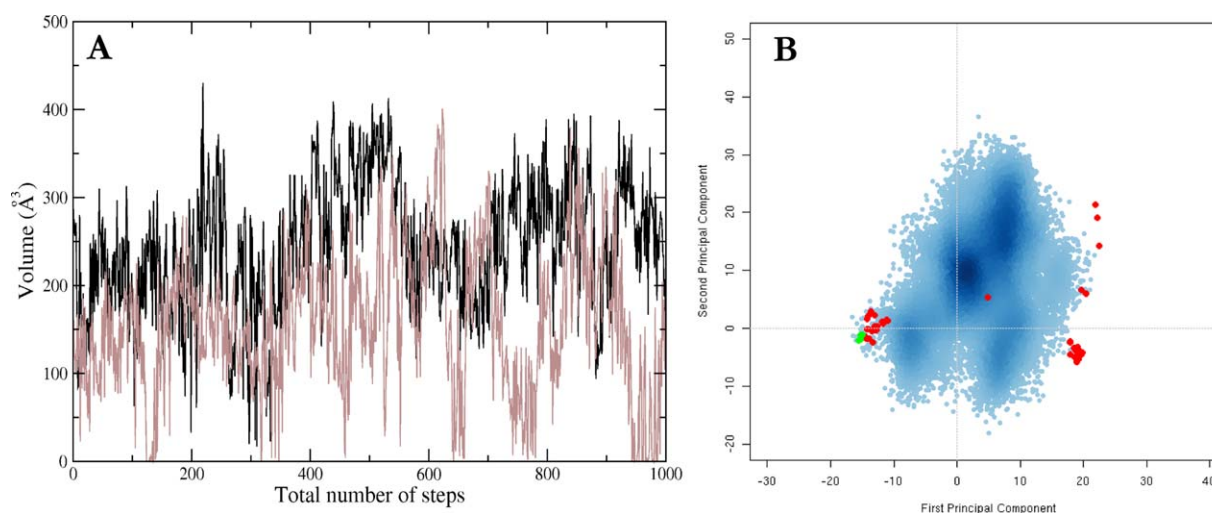
Figure 5. Channel volume (A) and PC analysis (B) during MD simulations for the apo TcUGM. Two independent simulations were superimposed in the analysis (black and brown series). PC analysis space built using all the AfUGM (red dots) and TcUGM (green dots) crystal structures. Dark regions in the PC space correspond to more populated configurations.

first one; that is, the channel widely opens and remains open during the time scale of the simulation (data not shown). Large fluctuations, with a deviation of the volume values greater than 70 Å^3 in the channel size were observed in all the independent simulations (Fig. 4A). The holo state, on the other hand, maintains the closed channel conformation as observed in the substrate-bound crystal structure (Fig. 4C), with the channel volume values around $20 \pm 15 \text{ Å}^3$.

PC analysis of the apo UGM dynamics (Fig. 4B) also supports a separation of conformations based on the opening of the channel, as the enzyme projection moves from the substrate-bound conformation (PC1 ~ -13) toward the substrate-free conformation (PC1 ~ 10). There is a highly populated region at PC1 ~ -7 that corresponds to the simulation mentioned above in which the 170s flap closes into a conformation distinct from that of the crystal structure after opening. PC analysis of the holo UGM confirms its stability in the closed state since the only populated region is observed around PC1 ~ -13 (Fig. 4D).

Conventional all-atom MD simulation time scales may not be adequate to observe all the relevant transitions. Accelerated MD (aMD) simulations have emerged as one of the alternatives to simulate low-frequency conformational transitions. The PC analysis, which was done using all the AfUGM structures, suggested additional configuration space along PC2 that was not explored in conventional MD simulations (Fig. 4B). For that reason, aMD simulations of the apo TcUGM were performed to further explore the configurational space of the system. Consistent with the MD simulations, an opening event was observed at the very beginning of the apo aMD simulations. Similar to one of the two independent MD simulations of the apo UGM several

opening and closing transitions of the 170s flap were observed during the aMD simulations (Fig. 5A). As observed in MD simulations, the 170s flap closes into a different conformation than that of the crystal structure. Figure 5B shows that aMD greatly augments sampling achieved by conventional MD, since PC2 was also explored extensively. Both minima at PC1 ~ -13 and PC1 ~ -7 observed in MD simulations were also explored in aMD, although various new regions were also extensively explored.

The influence of the substrate on TcUGM dynamics

To address which part of the substrate specifically controls the channel behavior, simulations of the enzyme complexed with the substrate fragments UDP and uridine were performed.

MD simulations of UGM with UDP bound show a less stable channel compared to the holo state. The channel of UGM with UDP bound opens during the two independent simulations and reaches volumes of $150 \pm 35 \text{ Å}^3$ and $110 \pm 30 \text{ Å}^3$ at the end of the simulations (Fig. 6A). The larger volume corresponds to an opening event of the 200s flap (Fig. 7B) observed at the end of this individual simulation. The 170s flap remains stable during the time scale of both simulations (Fig. 7B). PC analysis of UDP bound shows a larger explored space, evidencing some distortion in the channel compared with the holo case (Fig. 6B).

When the diphosphate moiety is also absent, as in the URI complex simulation, the 200s flap opens at the very beginning of the simulations and increases the volume of the channel toward 130 ± 40 Å^3 (Fig. 6C). As observed in the UDP-bound case, the 170s flap remains closed in both independent simulations (Fig. 7C). PC analysis indicates that the URI-bound UGM explores a minimum at PC1 ~ 5
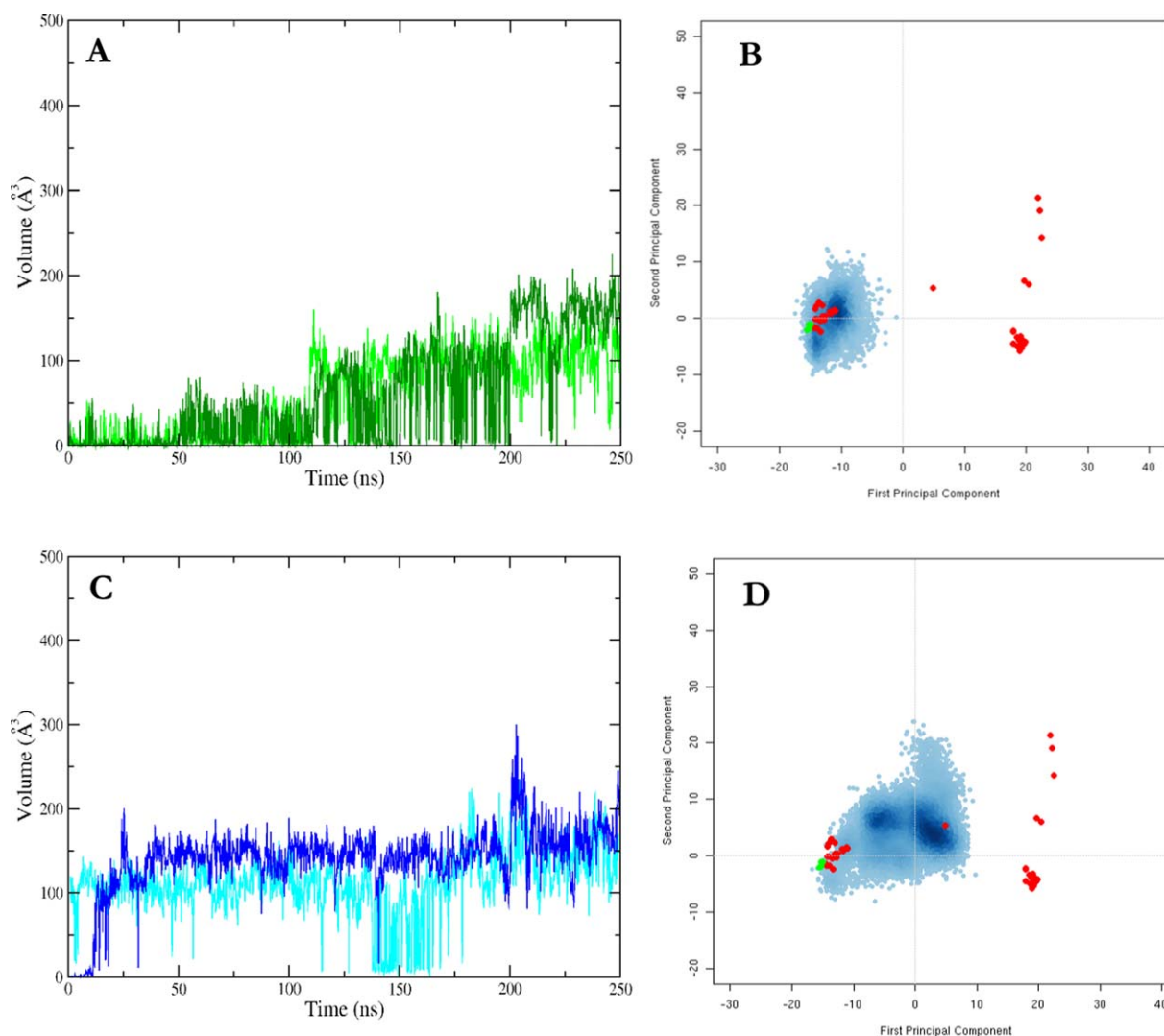
Figure 6. Channel volume and PC analysis for two independent MD simulations of the UDP-bound (A and B, respectively) and uridine-bound (C and D respectively) *Tc*UGM. Two MD simulations were superimposed for the channel volume analysis in both the UDP-bound (A) and the uridine-bound (C) enzyme (independent simulations shown as green and light green series in Panel A, blue and light blue series in Panel B). PC space built using all the AfUGM (red dots) and TcUGM (green dots) crystal structures. Dark regions in the PC space correspond to more populated configurations.

and another one at PC1∼−5, thus moving through PC1 toward the open conformation. Accelerated MD simulations also supported the trends in the classical MD simulations (data not shown). The URI-bound channel thus does not resemble that of the apo state in neither the cavity volume calculations, nor in the PC analysis, suggesting that the uridine moiety plays an important role in maintaining the channel structure.

The results mentioned above also indicate that the Gal*p* and diphosphate moieties contribute to the stabilization of the closed conformation by controlling the 200s flap movement. Because the two independent simulations of the UDP-bound case display increasing trends in the channel volume, no conclusive conclusions can be made from the UDP-bound case.

In summary, the holo form, with the co-crystallized natural substrate, does not result in any distortion in the flaps (Fig. 7A). When the Gal*p* moiety is not present, as in the UDP-bound enzyme, some perturbations were observed in the 200s flap (Fig. 7B). When the diphosphate moiety is also absent, as in the uridine-bound enzyme, the 200s flap undergoes a clear opening whereas the 170s flap maintains its holo-like conformation (Fig. 7C). Only in the apo state do both the 200s and 170s flaps undergo large distortions (Fig. 7D), highlighting the role of the uridine moiety in regulating the aperture of the 170s flap.

Electrostatic network in the active site
Considering that the opening events could be crucial for enzymatic activity, the behavior of active site residues will be described. The residues Arg176 and
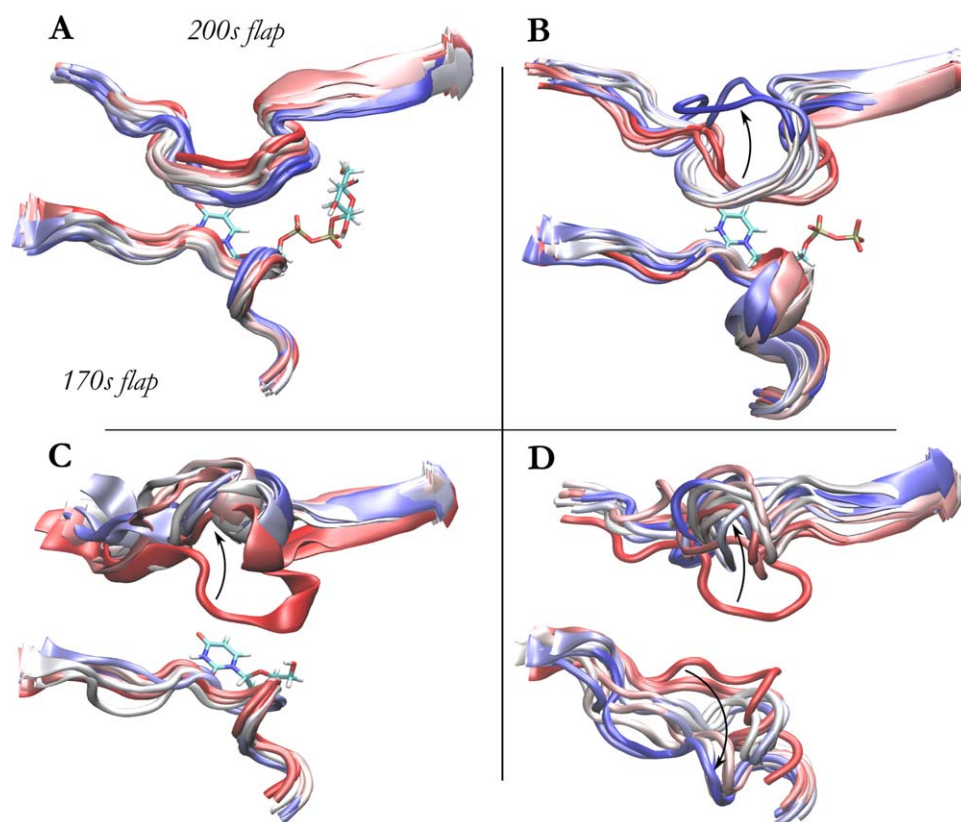
Substrate-Dependent Dynamics of UGM

Figure 7. The 170s and 200s flaps during MD simulations for the four systems studied: UDP-Galp-bound (A), UDP-bound (B), uridine-bound (C), and apo enzyme (D). Snapshots are colored according to timestep, on a red-white-blue color scale. Arrows show the direction of the flaps displacement during the simulations.

Asn201 belonging to the 170s and 200s flaps, respectively, interact mainly with the Galp moiety and, to a lesser extent, with the diphosphate group (Fig. 8). Other active site residues, such as Tyr317, Tyr34, Tyr429, and Arg327, interact only with the diphosphate moiety, as observed in crystal structures.[8] There are a few active site residues, including Phe102, Gln103, and Ala178, which form a strong hydrogen bond network with the uridine moiety of the ligand. Those residues that interact with both ligand moieties Galp and Uridine undergo high fluctuations when the ligand is removed (Fig. 8, right panels). On the other hand, residues that interact specifically with the diphosphate moiety remain stable even in the absence of the ligand (Fig. 8—middle panels).

We also note that in the opening process hydrogen bonds between Glu175 (from 170s flap) with both Gly466 (from 460s flap) and His67 break regardless of the protonation/tautomeric state of His67. These three residues form a latch that helps both the 170s and 460s flaps maintain the closed conformation.

Site-directed mutagenesis

Site-directed mutagenesis and kinetic assays were used to examine the hypothesis proposed by the simulations that interactions with the substrate diphosphate group are particularly important for stabilizing the closed active site. Residues of TcUGM that directly interact with the diphosphate group in the TcUGM-UDP crystal structure or that are predicted to interact with the diphosphate of UDP-Galp were mutated: R176A, R327A, Y395F, Y429F, Y317F. The steady-state kinetic constants for these variants are listed in Table II. Three of the targeted residues are clearly important for efficient catalysis: Arg176, Tyr395, and Tyr317. Mutation of these three residues individually decreases efficiency (k_{cat}/K_M) by a factor of 30–500. Arg176 is clearly the most important of these residues according to the kinetic data. Mutation of Arg176 to Ala decreases the catalytic efficiency by a factor of over 500, primarily by decreasing k_{cat}. This residue was observed to interact directly with the reactive moiety of the substrate Galp, and it is located on of one of the mobile flaps. These experimental results support the hypothesis developed from the calculations that diphosphate recognition is a key for maintaining the closed state during catalysis.

Discussion

The simulations revealed new aspects of active site flexibility in eukaryotic UGMs that were not evident from the crystal structures. For example, the crystal structures of apo and substrate-bound AfUGM
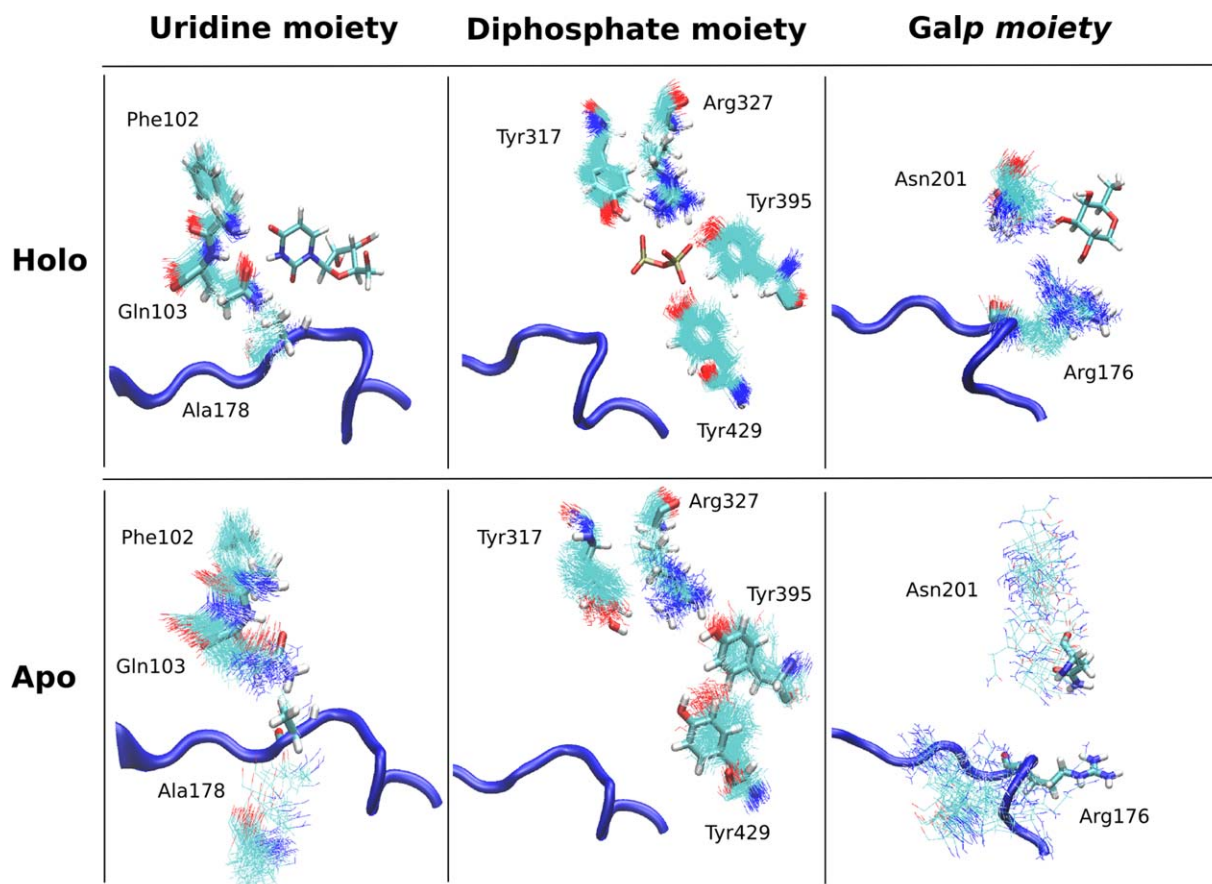
Figure 8. Molecular details of the active site residues for the holo (top panel) and apo (bottom panel) enzyme. Multiple snapshots during MD simulations were superimposed to provide qualitative information about the flexibility of the residues. The figure was divided based on the three moieties of the substrate, only for clarification purposes: uridine (left), diphosphate (middle), and Gal*p* (right) moieties. The 170s flap is included in every subdivision as a point of reference (blue). [Color figure can be viewed in the online issue, which is available at wileyonlinelibrary.com.]

implied that there are two mobile flaps, the 170s flaps and the 200s flaps, that together close or open upon substrate binding or product release, respectively. The simulations show that the substrate-free TcUGM adopts the open conformation observed in the other eukaryotic UGM from *A. fumigatus*. The channel seems to be large enough to be used by the substrate to reach the active site. Interestingly, the MD simulations revealed a third mobile loop consisting of residues 462–469. This loop contains the Gly466 that interacts with Glu175 and His67. Thus, the simulations suggest that an additional mobile loop functions in substrate recognition of

TcUGM and presumably other eukaryotic UGMs such as AfUGM. The motion of this loop will need to be considered in inhibitor design strategies.

The MD simulations provide the first clues about the minimum molecular fragment needed to stabilize the closed conformation of the active site, which is particularly important for planning fragment-based inhibitor design. In this sense, a direct relationship between the molecular moieties of the ligand and the flaps involved in the opening and closing of the enzyme are proposed: Gal*p*, and more importantly Gal*p* + diphosphate controls the 200s flaps, most likely via Asn201. The uridine

Table II. *Steady-State Kinetic Constants for TcUGM and TcUGM Mutant Enzymes*

Protein	k_{cat} (s^{-1})	K_M (µM)	k_{cat}/K_M (s^{-1} M^{-1})	Relative $(k_{cat}/K_M)^a$
TcUGM[a]	13.4 ± 0.3	140 ± 10	93 ± 6	1.0 ± 0.1
R176A	0.0223 ± 0.0003	134 ± 6	0.167 ± 0.005	0.0018 ± 0.0001
R327A	4.2 ± 0.4	90 ± 30	47.1 ± 13.8	0.5 ± 0.2
Y395F	0.247 ± 0.037	91 ± 49	2.7 ± 1.5	0.03 ± 0.02
Y429F	6.29 ± 0.14	100 ± 7	63 ± 5	0.68 ± 0.07
Y317F	0.290 ± 0.013	334 ± 38	0.87 ± 0.1	0.009 ± 0.001

Data from Oppenheimer *et al.*[36]
[a] ($k$cat/KM of mutant)/($k$cat/KM of TcUGM).
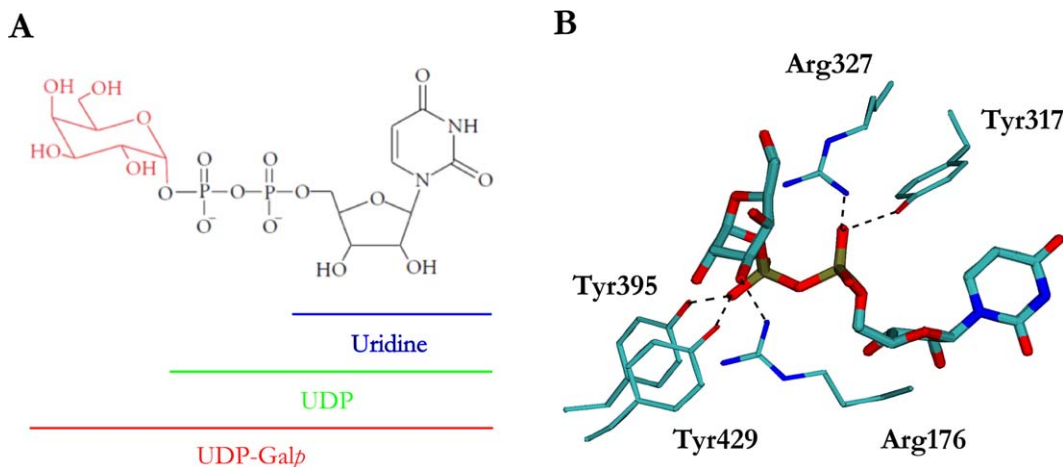
Substrate-Dependent Dynamics of UGM

Figure 9. (A) Chemical structure of UDP-Galp substrate and the truncated substrates used in the simulations. (B) Active site of TcUGM highlighting the residues targeted for site-directed mutagenesis. [Color figure can be viewed in the online issue, which is available at wileyonlinelibrary.com.]

moiety, on the other hand controls the 170s flap through a hydrogen bonding network between Phe102, Gln103, and Ala178. Interestingly, the 170s flap residue Arg176 is not able to control the 170s flap opening, because when the interaction between Arg176 and the substrate disappear, as in the truncated uridine substrate, the 170s flap remains stable during the time scale of the simulation.

Mutation of Arg176 sharply decreases the catalytic efficiency, a fact that could be related to the direct interaction between the residue and Galp, as observed in the simulations. Several opening and closing transitions were observed during the aMD simulations of apo TcUGM, implying that the flaps are flexible in the absence of the substrate. The simulation results are thus consistent with conformational selection as a plausible mechanism for substrate binding.[17]

These results place constraints on inhibitor design. In particular, potent inhibitors will likely need to engage the residues that interact with the diphosphate group of the substrate to stabilize the closed active site channel conformation, and thus diphosphate mimics are desirable components of libraries used for fragment-based screening of eukaryotic UGMs. Accelerated MD simulations allow us to sample larger configurational space, suggesting new allosteric binding sites for drug discovering.

Conclusions

By performing classical and accelerated MD simulations, we found an ensemble of conformations for the unsolved structure of apo TcUGM, which is of great importance in our drug design efforts. Our results support the suspected correlation between the presence of the substrate and the open/closed conformational equilibrium of the enzyme. More specifically, we identify that the Galp and diphosphate ligand moieties seem to control the 200s flap, whereas the uridine moiety seems to regulate the aperture of the 170s flap.

Methods

System preparation

Different TcUGM systems were built to be used in MD and accelerated MD simulations: (i) TcUGM with no substrate (apo), (ii) TcUGM with the natural substrate UDP-Galp, (iii) TcUGM with a truncated substrate, UDP, in which the galactopyranose was excluded from UDP-Galp, and (iv) TcUGM with uridine bound, excluding both the galactopyranose and diphosphate moiety (Fig. 9).

The crystal structure of the reduced TcUGM (PDB ID 4DSH) co-crystallized with the truncated substrate (UDP) in the active site was used to build the systems. The coordinates needed to complete the natural substrate were taken from the crystal structure of AfUGM (PDB ID 3UTH). All histidine protonation states were assigned based on the immediate environment in the crystal structures, and cross-checked against the protonation prediction server H++.[18] All histidines maintained the same immediate environments validating the choice of protonation states. Two histidines had particularly high predicted pK_a values and were assumed protonated (His62 and His67).

The Amber ff99SB force field[19] with explicit TIP3P[20] water molecules was used in all simulations. The minimum distance between the protein and the water box edge was 12Å. Crystallographic waters were retained as found in the original crystal structures. The FADH$^-$ and the substrate parameters were taken from GLYCAM.[21]

Molecular dynamics simulations

MD simulations were performed using the pmemd module within the AMBER11 simulation package. Periodic boundary conditions and Ewald sums were employed for the long-range electrostatic interactions.[20] The SHAKE algorithm,[22] and a 2 fs time
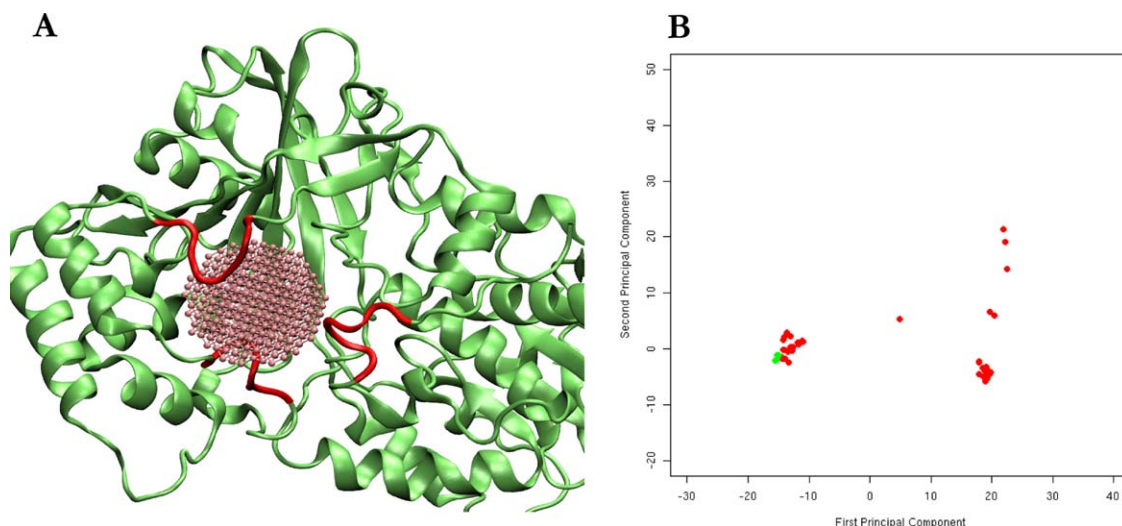
Figure 10. (A) Cartoon representation of the sphere used to estimate the volume of the tunnel using POVME software.[34] The flaps surrounding the tunnel are highlighted in red. (B) PC analysis space built using all the AfUGM (red) and TcUGM (green) crystal structures. PC1 adequately discriminates between holo (PC1 $\sim$ −12) or free enzyme (PC1 $\sim$ 20). There is an intermediate state at PC1 $\sim$ 5 which corresponds to the H subunit of an AfUGM structure (PDB ID 3UKH). [Color figure can be viewed in the online issue, which is available at wileyonlinelibrary.com.]

step were used for the propagation of coordinates in time in the NPT ensemble, using the Berendsen thermostat and barostat.[23] The equilibration process was performed by slowly heating the system from 0 to 300 K over the course of 500 ps. We performed triplicate 200 ns simulations of apo UGM, and duplicate 250 ns simulations for each of the UDP-Gal*p*-, UDP-, and uridine-bound states.

Accelerated MD

All-atom molecular dynamics simulations have been widely used to study protein conformations with great success. The time scale of the simulations, however, is not always sufficient to sample accurately the relevant configurational space of the protein. This problem can be overcome through the use of enhanced sampling methods, including the use of implicit solvent, assigning a higher temperature to the system, applying an artificial randomly oriented force to the substrate, and using a guide force that helps the system visit high energy configurations.[24–28] Another approach, known as accelerated MD (aMD), modifies the classical potential energy $V(r)$ by adding a bias potential $\Delta V(r)$ depending on a pre-defined threshold potential energy E and a tuning parameter α that determines how deeply the original potential energy will be modified,[29] as shown in Eqs. (1) and (2) below:

$$V'(r) = \begin{cases} V(r), & V(r) \geq E \\ V(r) + \Delta V(r), & V(r) < E \end{cases} \quad (1)$$

$$\Delta V(r) = \frac{(E - V(r))^2}{\alpha + (E - V(r))} \quad (2)$$

where $V'(r)$ is the modified potential. The aMD approach is especially attractive because it does not

require a priori knowledge of the reaction path. This technique has been successfully used during the last years by our group to sample conformational changes occurring on the micro- to milli-second time scales.[30–33]

Both total potential energy V_{total} and dihedral potential energy V_{dihed} were modified during MD simulations. The parameters for V_{total} (E_{total} and α_{total}) and for V_{dihed} (E_{dihed} and α_{dihed}) were calculated using Eqs. (3) and (4) as suggested in previous works[32]:

$$E_{total} = \langle V_{total} \rangle + \alpha_{total}$$
$$\alpha_{total} = \frac{7}{40} n_{atom} \quad (3)$$

$$E_{dihed} = \langle V_{dihed} \rangle + \alpha_{dihed} * 5$$
$$\alpha_{dihed} = \frac{4}{5} n_{res} \quad (4)$$

where n_{atom} and n_{res} correspond to the total number of atoms and residues, respectively. The average total potential $\langle V_{total} \rangle$ and dihedral $\langle V_{dihed} \rangle$ potential energies were extracted from a 10 ns of classics MD simulation.

Analysis tools

The volume of the tunnel was computed using the software POcket Volume Measurer (POVME),[34] which computes the free space within a pre-defined selected sphere. In this case the sphere was large enough to just include the tunnel, but not the active site, making the volume a good comparative metric of the accessibility through this tunnel (Fig. 10A). Different sphere parameters (radius, center etc.) result in different estimates for the volume, however, the same trends are conserved.

PC analysis was performed using Bio3d package.[35] PC space was built by using all the available crystal structures of eukaryotic UGM: 56 belong to all the crystallized subunits of *Af*UGM in both holo and apo forms and 2 belong to the holo state of TcUGM (Fig. 10B). It should be noted that PC1 discriminates very well between the apo state (PC1~20) and the holo state (PC1~ −12) (Fig. 10B). The first 50 ns of each MD simulation were not considered in PC analysis.

Enzyme activity studies

Site-directed mutants of TcUGM (Table II) were created using the QuikChange Site-Directed Mutagenesis Kit (Stratagene) and verified by DNA sequencing. The mutant enzymes were expressed and purified as described previously.[36] Kinetic constants were determined using steady-state assays as described previously.[36,37] Briefly, the rate of reverse reaction of UDP-Gal*f* to UDP-Gal*p* was measured at 37°C and pH 7.5 in the presence of 20 mM dithionite. The reverse reaction was used because the equilibrium between UDP-Gal*p* and UDP-Gal*f* favors UDP-Gal*p* by the ratio of 13:1.

Acknowledgment

References

1. Silveira A, Segura E, Guillén G, Pinto Díaz J, Lorca M, Schenone H, Valdés J, Rojas de Arias A, Russomando G, Salvatella R (2001) Chagas Control in the Southern Cone Countries: history of an International Initiative, 1991/2001. Available at: http://www.paho.org/English/AD/DPC/CD/dch-historia-incosur.htm.

2. Caldas IS, da Matta Guedes PM, dos Santos FM, de Figueiredo Diniz L, Martins TAF, da Silva do Nascimento AF, Azevedo MA, de Lima WG, Neto RMN, Torres RM et al (2013) Myocardial scars correlate with eletrocardiographic changes in chronic Trypanosoma cruzi infection for dogs treated with Benznidazole. Trop Med Intl Health 18:75–84.

3. Lederkremer RM, Agusti R (2009) Glycobiology of Trypanosoma cruzi. Adv Carbohydr Chem Biochem 62: 311–366.

4. Kizjakina K, Tanner JJ, Sobrado P (2013) Targeting UDP-galactopyranose mutases from eukaryotic human pathogens. Curr Pharm Des 19:2591–2573.

5. Sobrado P (2012) Noncanonical reactions of flavoenzymes. Int J Mol Sci 13:14219–14242.

6. Sanders DAR, Staines AG, McMahon SA, McNeil MR, Whitfield C, Naismith JH (2001) UDP-galactopyranose mutase has a novel structure and mechanism. Nature Struct Mol Biol 8:858–863.

7. Dhatwalia R, Singh H, Oppenheimer M, Karr DB, Nix JC, Sobrado P, Tanner JJ (2012) Crystal structures and small-angle x-ray scattering analysis of UDP-galactopyranose mutase from the pathogenic fungus Aspergillus fumigatus. J Biol Chem 287:9041–9051.

8. Dhatwalia R, Singh H, Oppenheimer M, Sobrado P, Tanner JJ (2012) Crystal structures of Trypanosoma cruzi UDP-galactopyranose mutase implicate flexibility of the histidine loop in enzyme activation. Biochemistry 51:4968–4979.

9. Karunan Partha S, Sadeghi-Khomami A, Cren S, Robinson RI, Woodward S, Slowski K, Berast L, Zheng B, Thomas NR, Sanders DAR (2011) Identification of novel inhibitors of UDP-galactopyranose mutase by structure-based virtual screening. Mol Inform 30:873–883.

10. Carlson EE, May JF, Kiessling LL (2006) Chemical probes of UDP-galactopyranose mutase. Chem Biol 13: 825–837.

11. Dykhuizen EC, Kiessling LL (2009) Potent ligands for prokaryotic UDP-galactopyranose mutase that exploit an enzyme subsite. Org Lett 11:193–196.

12. Dykhuizen EC, May JF, Tongpenyai A, Kiessling LL (2008) Inhibitors of UDP-galactopyranose mutase thwart mycobacterial growth. J Am Chem Soc 130: 6706–6707.

13. Scherman MS, Winans KA, Stern RJ, Jones V, Bertozzi CR, McNeil MR (2003) Drug targeting Mycobacterium tuberculosis cell wall synthesis: development of a microtiter plate-based screen for UDP-galactopyranose mutase and identification of an inhibitor from a uridine-based library. Antimicrob Agents Chemother 47:378–382.

14. Borrelli S, Zandberg WF, Mohan S, Ko M, Martinez-Gutierrez F, Partha SK, Sanders DAR, Av-Gay Y, Pinto BM (2010) Antimycobacterial activity of UDP-galactopyranose mutase inhibitors. Int J Antimicrob Agents 36:364–368.

15. Completo GC, Lowary TL (2008) Synthesis of galactofuranose-containing acceptor substrates for mycobacterial galactofuranosyltransferases. J Org Chem 73:4513–4525.

16. Richards MR, Lowary TL (2009) Chemistry and biology of galactofuranose-containing polysaccharides. Chembiochem 10:1920–1938.

17. Grant BJ, Gorfe AA, McCammon JA (2010) Large conformational changes in proteins: signaling and other functions. Curr Opin Struct Biol 20:142–147.

18. Gordon JC, Myers JB, Folta T, Shoja V, Heath LS, Onufriev A (2005) H++: a server for estimating pKas and adding missing hydrogens to macromolecules. Nucleic Acids Res 33:W368–371.

19. Hornak V, Abel R, Okur A, Strockbine B, Roitberg A, Simmerling C (2006) Comparison of multiple Amber force fields and development of improved protein backbone parameters. Proteins 65:712–725.

20. Jorgensen WL, Chandrasekhar J, Madura JD, Impey RW, Klein ML (1983) Comparison of simple potential functions for simulating liquid water. J Chem Phys 79: 926.

21. Kirschner KN, Yongye AB, Tschampel SM, González-Outeiriño J, Daniels CR, Foley BL, Woods RJ (2008) GLYCAM06: a generalizable biomolecular force field. Carbohydrates. J Comput Chem 29:622–655.

22. Ryckaert J-P, Ciccotti G, Berendsen H (1977) Numerical integration of the cartesian equations of motion of a system with constraints: molecular dynamics of n-alkanes. J Comp Phys 23:341,327.

23. Berendsen HJC, Postma JPM, Van Gunsteren WF, DiNola A, Haak JR (1984) Interaction models for water in relation to protein hydration. J Chem Phys 18:3684–3690.

24. Torrie GM, Valleau JP (1977) Nonphysical sampling distributions in Monte Carlo free-energy estimation: umbrella sampling. J Comp Phys 23:187–199.
25. Sugita Y, Okamoto Y (1999) Replica-exchange molecular dynamics method for protein folding. Chem Phys Lett 314:141–151.
26. Wu X, Wang S (1999) Enhancing systematic motion in molecular dynamics simulation. J Chem Phys 110: 9401–9410.
27. Banushkina P, Meuwly M (2005) Free-energy barriers in MbCO rebinding. J Phys Chem B 109:16911–16917.
28. Crespo A, Martí MA, Estrin DA, Roitberg AE (2005) Multiple-steering QM-MM calculation of the free energy profile in chorismate mutase. J Am Chem Soc 127:6940–6941.
29. Hamelberg D, Mongan J, McCammon JA (2004) Accelerated molecular dynamics: a promising and efficient simulation method for biomolecules. J Chem Phys 120: 11919–11929.
30. De Oliveira CAF, Hamelberg D, McCammon JA (2007) Estimating kinetic rates from accelerated molecular dynamics simulations: alanine dipeptide in explicit solvent as a case study. J Chem Phys 127: 175105.
31. Bucher D, Pierce LCT, McCammon JA, Markwick PRL (2011) On the use of accelerated molecular dynamics to enhance configurational sampling in ab initio simulations. J Chem Theory Comput 7:890–897.
32. Wereszczynski J, McCammon JA (2012) Accelerated molecular dynamic in computational drug design. Methods Mol Biol 819:515–524.
33. Hamelberg D, Shen T, McCammon JA (2005) Relating kinetic rates and local energetic roughness by accelerated molecular-dynamics simulations. J Chem Phys 122:241103.
34. Durrant JD, de Oliveira CAF, McCammon JA (2011) POVME: an algorithm for measuring binding-pocket volumes. J Mol Graph Model 29:773–776.
35. Grant BJ, Rodrigues APC, ElSawy KM, McCammon JA, Caves LSD (2006) Bio3d: an R package for the comparative analysis of protein structures. Bioinformatics 22:2695–2696.
36. Oppenheimer M, Valenciano AL, Kizjakina K, Qi J, Sobrado P (2012) Chemical mechanism of UDP-galactopyranose mutase from Trypanosoma cruzi: a potential drug target against Chagas' disease. PLoS ONE 7:e32918.
37. Oppenheimer M, Poulin MB, Lowary TL, Helm RF, Sobrado P (2010) Characterization of recombinant UDP-galactopyranose mutase from Aspergillus fumigatus. Arch Biochem Biophys 502:31–38.
38. Van Straaten KE, Routier FH, Sanders DAR (2012) Structural insight into the unique substrate binding mechanism and flavin redox state of UDP-galactopyranose mutase from Aspergillus fumigatus. J Biol Chem 287:10780–10790.